Ultralow 1/f noise in epigraphene devices

Applied Physics Letters

RESEARCH ARTICLE | FEBRUARY 27 2024

Ultralow 1/f noise in epigraphene devices

N. Shetty ✉ ; F. Chianese ; H. He ; J. Huhtasaari ; S. Ghasemi ; K. Moth-Poulsen ; S. Kubatkin ; T. Bauch ; S. Lara-Avila

Appl. Phys. Lett. 124, 093503 (2024)
https://doi.org/10.1063/5.0185890

AIP Publishing

Applied Physics Letters ARTICLE pubs.aip.org/aip/apl

Ultralow 1/f noise in epigraphene devices

Cite as: Appl. Phys. Lett. **124**, 093503 (2024); doi: 10.1063/5.0185890
Submitted: 2 November 2023 · Accepted: 24 January 2024 ·
Published Online: 27 February 2024

View Online Export Citation CrossMark

N. Shetty,[1,a] F. Chianese,[1] H. He,[1,2] J. Huhtasaari,[1] S. Ghasemi,[3] K. Moth-Poulsen,[3,4,5,6] S. Kubatkin,[1] T. Bauch,[1] and S. Lara-Avila[1,7]

AFFILIATIONS

[1]Department of Microtechnology and Nanoscience, Chalmers University of Technology, 412 96 Gothenburg, Sweden
[2]RISE Research Institutes of Sweden, Box 857, S-50115 Borås, Sweden
[3]Department of Chemical Engineering, Universitat Politècnica de Catalunya, EEBE, Eduard Maristany 10-14, 08019 Barcelona, Spain
[4]Catalan Institution for Research & Advanced Studies, ICREA, Pg. Lluis Companys 23, Barcelona, Spain
[5]Institute of Materials Science of Barcelona, ICMAB-CSIC, Bellaterra, Barcelona 08193, Spain
[6]Department of Chemistry and Chemical Engineering, Chalmers University of Technology, Kemivägen 4, Gothenburg 412 96, Sweden
[7]National Physical Laboratory, Hampton Road, Teddington TW11 0LW, United Kingdom

[a]**Author to whom correspondence should be addressed:** snaveen@chalmers.se

ABSTRACT

We report the lowest recorded levels of $1/f$ noise for graphene-based devices, at the level of $S_V/V^2 = S_I/I^2 = 4.4 \times 10^{-16}$ (1/Hz), measured at $f = 10$ Hz ($S_V/V^2 = S_I/I^2 < 10^{-16}$ 1/Hz for $f > 100$ Hz) in large-area epitaxial graphene on silicon carbide (epigraphene) Hall sensors. This performance is made possible through the combination of high material quality, low contact resistance achieved by edge contact fabrication process, homogeneous doping, and stable passivation of the graphene layer. Our study explores the nature of $1/f$ noise as a function of carrier density and device geometry and includes data from Hall sensors with device area range spanning over six orders of magnitude, with characteristic device length ranging from $L = 1$ μm to 1 mm. In optimized graphene Hall sensors, we demonstrate arrays to be a viable route to improve further the magnetic field detection: a simple parallel connection of two devices displays record-high magnetic field sensitivity at room temperature, with minimum detectable magnetic field levels down to $B_{min} = 9.5$ nT/$\sqrt{\text{Hz}}$. The remarkable low levels of $1/f$ noise observed in epigraphene devices hold immense capacity for the design and fabrication of scalable epigraphene-based sensors with exceptional performance.

Two-dimensional (2D) materials have tremendous potential for a variety of sensing applications because faint stimuli (e.g., light, magnetic field, and chemical environment) can readily produce large changes in their electrical resistance. In particular, for graphene, its high carrier mobility, thermal conductivity, saturation velocity, and the ability to tune carrier density make this 2D material ideally suited for the implementation of sensors with resistive readout schemes in electronics,[1,2] chemical,[3] radiation,[4,5] and biological[6] applications. For practical sensors, however, the high sensitivity must be complemented with low-noise, to achieve signal-to-noise ratios (SNR) higher than unity. At low frequencies (DC), $1/f$ noise (also known as flicker noise, pink noise, or drift) is the main bottleneck to achieve high SNR.[1,7–9] Flicker noise, characterized by a spectral density $S(f) \sim 1/f^{\gamma}$ (where f represents frequency and $\gamma \approx 1$), is ubiquitous in many physical processes. For solid state devices including graphene, when a device is biased, the excess current noise can be written as fluctuations in electrical current: $\delta I \propto q(\delta N)\mu + qN(\delta\mu)$, where q is the charge of an electron, N is the number of charge carriers, and μ is the mobility. Thus, contribution to the noise could arise from fluctuations in number of charge carriers N[10–12] and/or fluctuation in mobility μ.[13–15] Specific to graphene, under theoretical conditions, it is possible to approach vanishing noise when graphene carrier density approaches zero (Dirac point), provided that, at effectively zero carrier concentration, the mobility of holes is similar to the mobility of electrons.[12,16–21] This is in general only possible at low temperatures, where suppressed thermal fluctuations enable approaching a zero-carrier density scenario. In practice, for graphene devices operating at room temperature, various approaches have been explored to reduce the contribution of $1/f$ noise, such as electron irradiation,[22] passivation with high-k dielectrics,[11,16] and low k dielectrics.[2] Yet, noise mitigation strategies are actively sought for graphene devices to optimize their performance.

To study noise in our devices, we have minimized all possible material-, device-, and instrumental-related noise sources. Since epitaxial growth of graphene involves annealing the SiC substrates at very

high temperatures, $T > 1800\,^{\circ}C$, crystal imperfections, vacancies, and thus, charge traps are considerably reduced.[5,23–26] Also, we have meticulously optimized the epitaxial growth parameters to obtain high-quality graphene on SiC resulting in an impressive reduction of bilayer (BL) graphene domains to a coverage <0.1% of the surface.[27,28] Our device fabrication incorporates an edge contact approach that consistently achieves contact resistance values below 50 $\Omega\cdot\mu$m.[29] Finally, to characterize noise, we employ a digital cross correlation spectrum analyzer to effectively eliminate instrumental noise.[30]

Figure 1(a) shows the Raman spectrum of optimized epigraphene on Si face (0001), as well as the SiC substrate. In epigraphene, the Raman spectrum contains information about both the graphene and interfacial carbon buffer layer. The buffer layer is characterized by a broad Raman band centered at approximately at 1355 cm^{-1}, which makes it hard to distinguish it from the (disorder) D peak (1360 cm^{-1}).[31] However, the absence of D′ ~1620 cm^{-1}, D + D′ ~2950 cm^{-1} (due to disorder), and the prominent 2D and 2D′ peaks suggest that the epigraphene layer is essentially defect-free.[32,33] Also visible in the spectrum is the D + D″ (also referred to as G*) at ~2500 cm^{-1}, which is identified purely for single layer graphene and disappears for increasing layer numbers.[33] To complement Raman studies, Fig. 1(b) shows the atomic force microscopy (AFM) topography image of epigraphene over a region of size $20 \times 20\,\mu m^2$. The surface is typically characterized by the presence of step edges with heights comparable to the unit cell height of 4H-SiC (≤1 nm).[34] Additionally, the phase-contrast AFM scan image Fig. 1(c) enables to distinguish monolayer (ML) from bilayer (BL) graphene domains; the light blue contrast represents very sparse BL domains, which are found mainly in regions with deep terrace formation during the growth process. In general, the surface study of our optimized material reveals that epigraphene has a regular surface morphology without gaps, and that growth of BL graphene domains is heavily suppressed. These characteristics result in a general reduction of the resistance anisotropy of the material and enable scalable patterning of the devices on the surface.

Figure 2 shows a representative transmission mode optical image of the Hall sensor devices patterned on epigraphene, having characteristic lengths of 1 μm and 1 mm. In the micrograph, metallic contacts appear black, while dark (light) shades of gray indicate the presence (absence) of epigraphene.[27] To achieve low contact resistance to epigraphene, we employed a specially designed tri-layer resist recipe, which creates edge contact between metal and graphene.[29] For these devices, contacts are formed by depositing a 5 nm thick titanium, followed by 100 nm Au as capping layer, using electron-beam evaporation. To explore the influence of device geometry on $1/f$ noise, we fabricated square-shaped devices with widths (w) of 1, 10, 100, and 1000 μm. Such wide range in device geometry is achievable due to large scale production of high-quality epigraphene as well as the scalable edge contact fabrication process.

To explore $1/f$ noise in epigraphene at different doping levels, we have utilized three strategies: chemical and electrostatic gating, molecular doping [F4TCNQ—2,3,5,6-tetrafluoro-tetracyanoquinodimethan and PMMA—poly(methyl-methacrylate)],[35] and polymer passivation (120 nm-thick PMMA layer). The latter serves as a control approach to benchmark the noise performance of the devices. First, we describe gated devices using a solid electrolyte implemented with lithium triflate (CF_3SO_3Li) diluted in a polyethylene glycol matrix in combination with a co-planar graphene electrode as gate. This approach allows gating epigraphene across Dirac point without degrading its mobility due to the absence of chemical interaction. Figure 3(a) shows a comparison of the resistance and noise power spectral density (PSD) (at $f = 10$ Hz) as a function of carrier density in a graphene Hall bar device. Each data point in noise PSD is a 30 min long measurement with minimum 100 spectral averages. The results

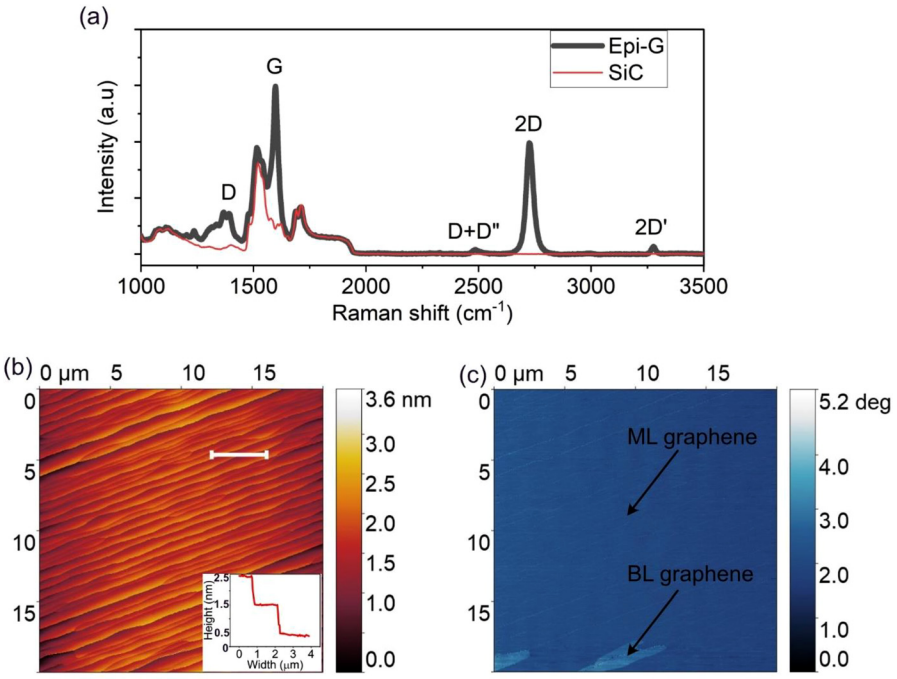

FIG. 1. (a) Raman spectrum of epigraphene (Epi-G) grown on 4H-SiC substrate (black) compared to the 4H-SiC substrate (red). (b) AFM height map of $20 \times 20\,\mu m^2$ area over a $7 \times 7\,mm^2$ epigraphene sample. The inset in (b) is the line profile of the height map, indicating the step height (≤1 nm) on the Si face of SiC substrate after the growth of epigraphene. (c) The AFM phase map of the same area as in (b). The light blue shaded patches at the bottom of the image indicate the BL graphene patches.

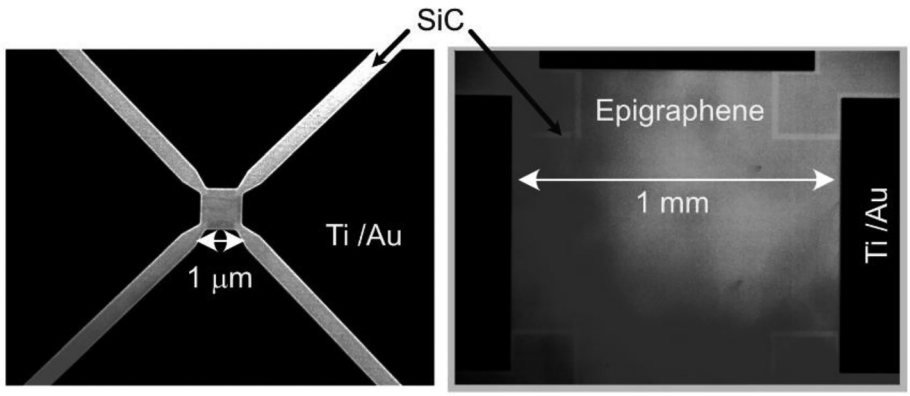

FIG. 2. Transmission mode optical image of 1 μm and 1 mm wide Hall sensor geometry fabricated using epitaxially grown graphene over the SiC substrate. Contacts are fabricated using edge contact fabrication process with 5 nm Ti and 100 nm Au.

confirm that epigraphene is intrinsically n-doped, with Dirac point located at about $V_g = -0.55$ V, and reveal that the maximum device noise ($S_V/V^2 = 7 \times 10^{-13}$ 1/Hz) occurs when electrostatic doping is in the vicinity of the Dirac point (for details of noise measurement setup see Fig. S1). This so-called "Λ" shape[20] of the noise spectrum can be attributed to the fact that, at 300 K, the epigraphene sample displays an uneven distribution of charge carriers around the charge neutrality point, forming electron–hole puddles resulting in potential (i.e., carrier density) fluctuations. To support this claim, the procedure to calculate disorder potential s is shown in Fig. S2 from the supplementary material. From this, the minimum attainable carrier density of epigraphene at room temperature is $|n_s| < 3 \times 10^{11}$ cm^{-2}, which yields an estimated disorder potential $s = 16$ meV. Thus, when the electrostatic gate is tuned to further reduce the carrier density in the material, the formation of electron–hole puddles manifests as a non-linear Hall (two-band model) coefficient.[2] Altogether, chemical and electrostatic doping of epigraphene reveals the low potential fluctuations in epigraphene ($s = 16$ meV), and that the lowest well-defined carrier density attainable in the material at room temperature is of the order of $|n| \approx 3 \times 10^{11}$ cm^{-2}. Higher carrier density levels result in decreased $1/f$ noise.

Having established the carrier density dependence of $1/f$ noise in epigraphene, we compare the noise performance of the different doping and passivation approaches. Figure 3(b) shows a comparison of noise power spectral density per unit area for epigraphene doped using the three different schemes, PMMA, F4TCNQ, and CF_3SO_3Li. The comparison shows that the solid electrolyte ($n = 0.4 \times 10^{12}$ cm^{-2}) used for gating the epigraphene displays the highest levels of noise, while molecular doping ($n = 0.42 \times 10^{12}$ cm^{-2}) and the PMMA-encapsulated device ($n = 7 \times 10^{12}$ cm^{-2}) show noise power amplitude about three orders of magnitude lower. While the high noise in chemically/electrostatically doped graphene could be attributed to mobile lithium ions causing carrier density fluctuations in epigraphene, the low noise in PMMA and F4TCNQ samples deserves more attention. This is because, with epigraphene exhibiting Λ shape in its PSD, the $1/f$ noise is expected to follow the empirical Hooge's law $\frac{S_V}{V^2} = \frac{S_I}{I^2} = \frac{S_R}{R^2} = \frac{\alpha_H}{Nf}$, where S_V, S_I, and S_R are the power spectral density (PSD) of the fluctuations in the values of voltage V, current I, and resistance R, N is the charge carrier number, f is the frequency, and α_H is the empirical Hooge parameter. With PMMA passivation resulting in heavily n-doped epigraphene, an order of magnitude higher than molecularly (F4TCNQ) doped epigraphene (see also tabulated data in supplementary material Table I), the small difference in noise amplitude results in different Hooge parameters for the different epigraphene doping. For PMMA samples at high doping, we obtain $\alpha_{H\text{-}PMMA} \approx 5 \times 10^{-4}$

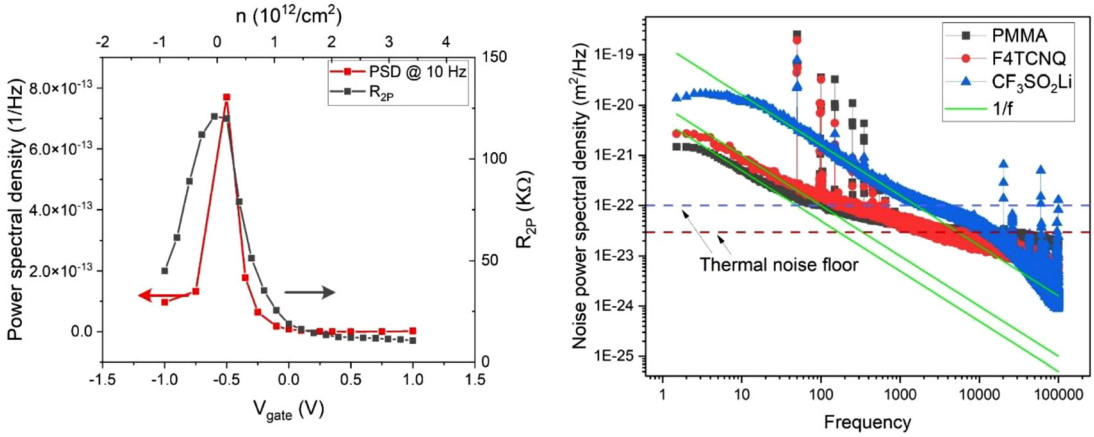

FIG. 3. (a) Comparison of two-point resistance (R_{2P}) and noise power spectral density amplitude (at f = 10 Hz) measured for electrolytically gated epigraphene. Negative charge carrier density corresponds to the p type of carrier. (b) Comparison of noise power spectral density (PSD) of PMMA ($n = 7 \times 10^{12}$ cm^{-2}), F4TCNQ ($n = 0.42 \times 10^{12}$ cm^{-2}), and CF_3SO_3Li ($n = 0.4 \times 10^{12}$ cm^{-2}). PSD is normalized with respect to device geometry. For CF_3SO_3Li, the values correspond to the gate voltage fixed at the Dirac point.

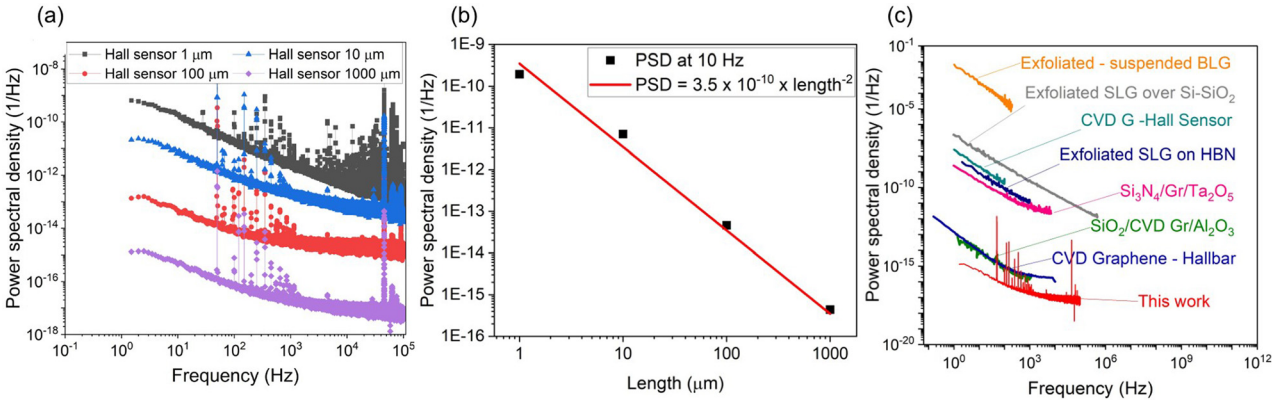

FIG. 4. (a) Noise PSD measured for device width varying from 1 to 1000 μm, within 2 to 100 kHz bandwidth. (b) Noise PSD measured at 10 Hz shows area dependency of noise PSD. (c) Comparison of noise PSD of epitaxial graphene (Epi-G) to historical data over wide variety of graphene devices. Observed noise in epitaxial graphene is an order lower than previously reported values.[11,16,17,30,36–38]

(see the supplementary material, Fig. S3), while for F4TCNQ, it can be as low as $\alpha_{\text{H-F4TCNQ}} \approx 10^{-5}$.[2]

We verify the geometrical scaling of noise anticipated by Hooge's law in devices of different sizes, spanning an area range from $A = 1$ to 10^6 μm^2. The total number of electrons N in a sample is related to the device size by the relation $N = l^2/(q\mu R)$, where l is the length of the sample, q is the elementary charge, μ is the mobility, and R is the sample resistance. Together with Hooge's law, the dependence of noise PSD over device geometry $S_V \propto 1/l^2$. Figure 4(a) illustrates the noise PSD measurements conducted on different PMMA-passivated epigraphene devices with varying $l = w$ ranging from 1 to 1000 μm (see supplementary material Table II for tabulated values of resistance, carrier density, and carrier mobility). As shown in Fig. 4(b), the variation in noise PSD $\propto a \times l^{-2}$ (where l is in units of μm) with the fitting coefficient a ranging from 3 to 5×10^{-10} (μm^2/Hz). Figure 4(c) shows a comparison of the PSD observed in large epigraphene devices, with noise reported for other types of graphene including exfoliated graphene, CVD-grown graphene, as well as graphene encapsulated by materials such as hBN, Ta_2O_5, and Al_2O_3 (for the area normalized comparison of PSDs see the supplementary material, Fig. S4). Remarkably, the noise PSD observed in our epigraphene devices is significantly lower compared to previously reported values in various graphene-based devices obtained from different sources.

Additionally, we demonstrate the implications of low noise in increasing the magnetic field sensitivity of Hall sensors, for which we arranged a parallel combination of sensors as shown in Fig. 5(a). At 20 kHz, the noise voltage measured in the parallel configuration of Hall sensors is about $1/\sqrt{2}$ that of the single device, resulting in a remarkable sensitivity of $B_{min} = V_N/(I_B R_H)$ (T/$\sqrt{}$Hz) = 9.5 nT/$\sqrt{}$Hz, setting a record for low sensitivity for graphene-based Hall sensors operating at room temperature.

In summary, the efforts here demonstrated for epigraphene optimization in terms of material and devices open the route for truly scalable graphene electronics. The unprecedented low levels of noise measured in our devices result from a combination of optimized epitaxial growth at very high temperature T > 1800 °C, the formation of low resistance ohmic contacts to epigraphene, and the uniform doping and passivation of devices. The scalability of epigraphene technology enables

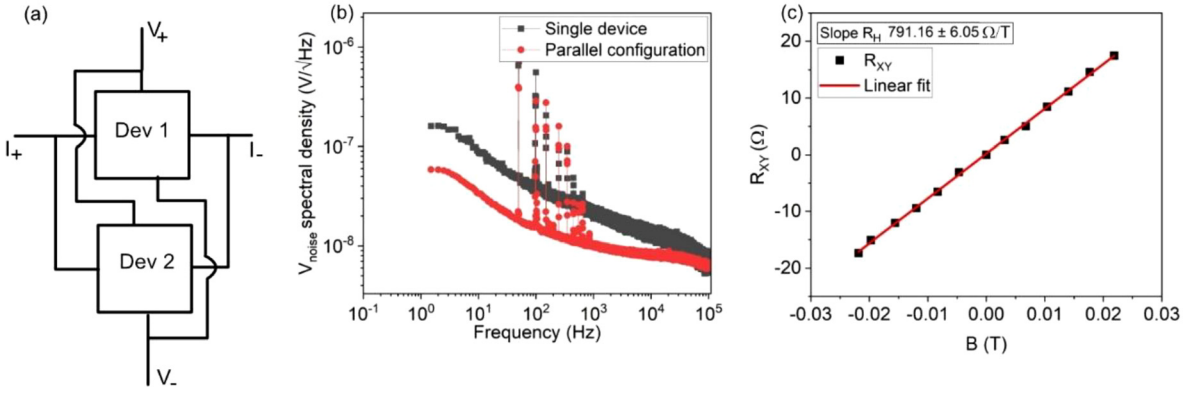

FIG. 5. (a) Parallel configuration of the two Hall sensors. (b) Comparison of noise voltage spectral density between single 1 mm Hall sensor and parallel configuration of two 1 mm Hall sensor devices as shown in (a). The voltage spectral density measured at $I = 400$ μA for both single and parallel configurations. Both the devices are doped with molecular dopant F4TCNQ, to tune the Fermi level near to the Dirac point. (c) Hall measurement of the parallel setup. Slope here represents the Hall coefficient $R_H \approx 791$ Ω/T. The data points are corrected for the thermal offset value.

us to design, fabricate, and test large area devices, a key requisite for increasing the complexity of future epigraphene electronics. Specifically, for Hall sensor devices, our results show that future array sensors could be a path toward decreasing the minimum detectable magnetic field that limits the Hall magnetometers. As a proof of concept, a simple parallel combination of sensors [Figs. 5(a)–5(c)] leads to a record low $B_{min} = V_N/(I_B R_H) = 9.5$ nT/$\sqrt{\text{Hz}}$ for graphene Hall magnetometers operating at room temperature. We foresee that fabrication of arrays is a feasible route to push down the limits of B_{min}, scaling down as $\sim 1/\sqrt{k}$, with k the number of interconnected Hall sensors. Our finding is instrumental in guiding the design of sensors utilizing scalable material growth and fabrication techniques, with the aim of minimizing the impact of noise and enhancing the sensitivity of the devices.

See the supplementary material for information on cross correlated noise measurement setup, calculation of disorder potential, Hooge parameter, and area normalized comparison of noise PSDs.

This work was jointly supported by the Swedish Foundation for Strategic Research (SSF) (Nos. GMT14-0077, RMA15-0024, and FFL21-0129), Chalmers Area of Advance Nano, Chalmers Area of Advance Energy, Chalmers Area of Advanced material, 2D TECH VINNOVA competence Center (Ref. 2019-00068), VINNOVA (Ref. 2020-04311 and 2021-04177), Marie Sklodowska-Curie grant QUESTech No. 766025, Knut and Alice Wallenberg Foundation (2019.0140), and the Swedish Research Council VR (Contract Nos. 2021-05252 and 2018-04962). This work was performed in part at Myfab Chalmers and Chalmers Materials Analysis Laboratory (CMAL).

AUTHOR DECLARATIONS

Conflict of Interest

The authors have no conflicts to disclose.

Author Contributions

Naveen Shetty: Conceptualization (equal); Data curation (lead); Formal analysis (lead); Investigation (lead); Methodology (lead); Resources (equal); Software (lead); Visualization (equal); Writing – original draft (lead); Writing – review & editing (equal). **F. Chianese:** Resources (equal); Writing – review & editing (supporting). **H. He:** Formal analysis (supporting); Supervision (supporting); Writing – review & editing (equal). **J. Huhtasaari:** Resources (equal); Writing – review & editing (supporting). **S. Ghasemi:** Writing – review & editing (supporting). **K. Moth-Poulsen:** Formal analysis (equal); Writing – review & editing (equal). **S. Kubatkin:** Conceptualization (supporting); Investigation (supporting); Supervision (supporting); Validation (supporting); Writing – review & editing (equal). **T. Bauch:** Conceptualization (equal); Formal analysis (supporting); Investigation (supporting); Software (supporting); Supervision (supporting); Visualization (equal); Writing – review & editing (supporting). **S. Lara-Avila:** Conceptualization (lead); Funding acquisition (equal); Methodology (equal); Supervision (lead); Validation (lead); Visualization (lead); Writing – review & editing (equal).

DATA AVAILABILITY

The data that support the findings of this study are available from the corresponding authors upon reasonable request.

REFERENCES

[1]H. Xu, L. Huang, Z. Zhang, B. Chen, H. Zhong, and L. M. Peng, "Flicker noise and magnetic resolution of graphene Hall sensors at low frequency," Appl. Phys. Lett. **103**(11), 112405 (2013).
[2]H. He, N. Shetty, T. Bauch, S. Kubatkin, T. Kaufmann, M. Cornils, R. Yakimova, and S. Lara-Avila, "The performance limits of epigraphene Hall sensors doped across the Dirac point," Appl. Phys. Lett. **116**(22), 223504 (2020).
[3]F. Yavari and N. Koratkar, "Graphene-based chemical sensors," J. Phys. Chem. Lett. **3**(13), 1746–1753 (2012).
[4]S. Lara-Avila, A. Danilov, D. Golubev, H. He, K. H. Kim, R. Yakimova, F. Lombardi, T. Bauch, S. Cherednichenko, and S. Kubatkin, "Towards quantum-limited coherent detection of terahertz waves in charge-neutral graphene," Nat. Astron. **3**(11), 983–988 (2019).
[5]H. He, N. Shetty, S. Kubatkin, P. Stadler, T. Löfwander, M. Fogelström, J. C. Miranda-Valenzuela, R. Yakimova, T. Bauch, and S. Lara-Avila, "Highly efficient UV detection in a metal-semiconductor-metal detector with epigraphene," Appl. Phys. Lett. **120**(19), 191101 (2022).
[6]Y. Liu, X. Dong, and P. Chen, "Biological and chemical sensors based on graphene materials," Chem. Soc. Rev. **41**(6), 2283–2307 (2012).
[7]N. A. Stutzke, S. E. Russek, D. P. Pappas, and M. Tondra, "Low-frequency noise measurements on commercial magnetoresistive magnetic field sensors," J. Appl. Phys. **97**(10), 10Q107 (2005).
[8]A. Polley, A. V. Ravichandran, V. S. Kumar, A. Venugopal, L. Cheng, A. T. Lucero, J. Kim, L. Colombo, and R. R. Doering, "Ambipolar gate modulation technique for the reduction of offset and flicker noise in graphene Hall-effect sensors," IEEE Sens. J. **21**(22), 25675–25686 (2021).
[9]T. Wang, D. Huang, Z. Yang, S. Xu, G. He, X. Li, N. Hu, G. Yin, D. He, and L. Zhang, "A review on graphene-based gas/vapor sensors with unique properties and potential applications," Nano-Micro Lett. **8**(2), 95–119 (2016).
[10]A. L. McWhorter and R. H. Kingston, *Semiconductor Surface Physics* (University of Pennsylvania Press, 1957).
[11]S. Peng, Z. Jin, D. Zhang, J. Shi, D. Mao, S. Wang, and G. Yu, "Carrier-number-fluctuation induced ultralow 1/*f* noise level in top-gated graphene field effect transistor," ACS Appl. Mater. Interfaces **9**(8), 6661–6665 (2017).
[12]I. Heller, S. Chatoor, J. Männik, M. A. G. Zevenbergen, J. B. Oostinga, A. F. Morpurgo, C. Dekker, and S. G. Lemay, "Charge noise in graphene transistors," Nano Lett. **10**(5), 1563–1567 (2010).
[13]A. Rehman, J. A. Delgado Notario, J. Salvador Sanchez, Y. M. Meziani, G. Cywiński, W. Knap, A. A. Balandin, M. Levinshtein, and S. Rumyantsev, "Nature of the 1/f noise in graphene—Direct evidence for the mobility fluctuation mechanism," Nanoscale **14**(19), 7242–7249 (2022).
[14]A. A. Balandin, "Review of the low-frequency 1/f noise in graphene devices," arXiv:1307.4797 (2013).
[15]R. P. Jindal and A. van der Ziel, "Model for mobility fluctuation 1/*f* noise," Appl. Phys. Lett. **38**(4), 290–291 (1981).
[16]Y. Wang, V. X. Ho, Z. N. Henschel, M. P. Cooney, and N. Q. Vinh, "Effect of high-κ dielectric layer on 1/*f* noise behavior in graphene field-effect transistors," ACS Appl. Nano Mater. **4**(4), 3647–3653 (2021).
[17]A. A. Balandin, "Low-frequency 1/*f* noise in graphene devices," Nat. Nanotechnol. **8**(8), 549–555 (2013).
[18]G. Xu, C. M. Torres, Y. Zhang, F. Liu, E. B. Song, M. Wang, Y. Zhou, C. Zeng, and K. L. Wang, "Effect of spatial charge inhomogeneity on 1/*f* noise behavior in graphene," Nano Lett. **10**(9), 3312–3317 (2010).
[19]Y. Zhang, E. E. Mendez, and X. Du, "Mobility-dependent low-frequency noise in graphene field-effect transistors," ACS Nano **5**(10), 8124–8130 (2011).
[20]P. Marconcini, "Model for 1/*f* noise in graphene and in more common semiconductors," Int. J. Circuits, Syst. Signal Process. **14**, 144–148 (2020).
[21]B. Pellegrini, "1/*f* noise in graphene," Eur. Phys. J. B **86**(9), 373 (2013).
[22]M. Z. Hossain, S. Rumyantsev, M. S. Shur, and A. A. Balandin, "Reduction of 1/*f* noise in graphene after electron-beam irradiation," Appl. Phys. Lett. **102**(15), 153512 (2013).
[23]M. E. Bathen, C. T. K. Lew, J. Woerle, C. Dorfer, U. Grossner, S. Castelletto, and B. C. Johnson, "Characterization methods for defects and devices in silicon carbide," J. Appl. Phys. **131**(14), 140903 (2022).
[24]C. Hettler, W. W. Sullivan, and J. Dickens, "Characterization of annealed HPSI 4H-SiC for photoconductive semiconductor switches," Mater. Sci. Forum **717–720**, 301–304 (2012).

[25]J. R. Jenny, D. P. Malta, V. F. Tsvetkov, M. K. Das, H. M. Hobgood, C. H. Carter, R. J. Kumar, J. M. Borrego, R. J. Gutmann, and R. Aavikko, "Effects of annealing on carrier lifetime in 4*H*-SiC," J. Appl. Phys. **100**(11), 113710 (2006).
[26]F. M. D. Pellegrino, G. Falci, and E. Paladino, "Charge carrier density noise in graphene: Effect of localized/delocalized traps," J. Stat. Mech. Theory Exp. **2019**(9), 094015.
[27]T. Yager, A. Lartsev, S. Mahashabde, S. Charpentier, D. Davidovikj, A. Danilov, R. Yakimova, V. Panchal, O. Kazakova, A. Tzalenchuk, S. Lara-Avila, and S. Kubatkin, "Express optical analysis of epitaxial graphene on SiC: Impact of morphology on quantum transport," Nano Lett. **13**(9), 4217–4223 (2013).
[28]G. R. Yazdi, T. Iakimov, and R. Yakimova, "Epitaxial graphene on SiC: A review of growth and characterization," Crystals **6**(5), 53 (2016).
[29]N. Shetty, H. He, R. Mitra, J. Huhtasaari, K. Iordanau, J. Wiktor, S. Kubatkin, S. P. Dash, R. Yakimova, L. Zeng, E. Olsson, and S. Lara-Avila, "Scalable fabrication of edge contacts to 2D materials: Implications for quantum resistance metrology and 2D electronics," ACS Appl. Nano Mater. **6**, 6292–6298 (2023).
[30]M. Marzano, A. Cultrera, M. Ortolano, and L. Callegaro, "A correlation noise spectrometer for flicker noise measurement in graphene samples," Meas. Sci. Technol. **30**(3), 035102 (2019).
[31]F. Fromm, M. H. Oliveira, Jr., A. Molina-Sánchez, M. Hundhausen, J. M. J. Lopes, H. Riechert, L. Wirtz, and T. Seyller, "Contribution of the buffer layer to the Raman spectrum of epitaxial graphene on SiC(0001)," New J. Phys. **15**(100), 043031 (2013).
[32]A. C. Ferrari and D. M. Basko, "Raman spectroscopy as a versatile tool for studying the properties of graphene," Nat. Nanotechnol. **8**(4), 235–246 (2013).
[33]A. Ben Gouider Trabelsi, F. V. Kusmartsev, A. Kusmartseva, F. H. Alkallas, S. Alfaify, and M. Shkir, "Raman spectroscopy imaging of exceptional electronic properties in epitaxial graphene grown on SiC," Nanomaterials **10**(11), 2234–2237 (2020).
[34]M. E. Levinshtein, S. L. Rumyantsev, and M. S. Shur, *Properties of Advanced Semiconductor Materials: GaN, AlN, InN, BN, SiC, SiGe* (Wiley, 2001).
[35]H. He, K. H. Kim, A. Danilov, D. Montemurro, L. Yu, Y. W. Park, F. Lombardi, T. Bauch, K. Moth-Poulsen, T. Iakimov, R. Yakimova, P. Malmberg, C. Müller, S. Kubatkin, and S. Lara-Avila, "Uniform doping of graphene close to the Dirac point by polymer-assisted assembly of molecular dopants," Nat. Commun. **9**(1), 3956 (2018).
[36]M. Kayyalha and Y. P. Chen, "Observation of reduced 1/f noise in graphene field effect transistors on boron nitride substrates," Appl. Phys. Lett. **107**(11), 113101 (2015).
[37]A. Porciatti, Z. Wang, P. Marconcini, G. Pennelli, G. Basso, D. Neumaier, and M. MacUcci, "Flicker noise in graphene-based Hall sensors," in International Conference on Noise and Fluctuations (ICNF), 2017.
[38]M. Kumar, A. Laitinen, D. Cox, and P. J. Hakonen, "Ultra low 1/*f* noise in suspended bilayer graphene," Appl. Phys. Lett. **106**(26), 263505 (2015).